Taylor & Francis
Taylor & Francis Group

ORIGINAL RESEARCH

🔓 OPEN ACCESS | Check for updates

Formyl peptide receptor-1 (FPR1) represses intestinal oncogenesis

Julie Le Naour[a,b,c], Léa Montégut[a,b,c], Yuhong Pan[a,b,d], Sarah Adriana Scuderi[a,b,e], Pierre Cordier[f], Adrien Joseph[a,b,c], Allan Sauvat[a,b], Valerio Iebba[g], Juliette Paillet[a,b,c], Gladys Ferrere[h], Ludivine Brechard[i], Claire Mulot[j], Grégory Dubourg[i], Laurence Zitvogel[c,k,l,m], Jonathan G. Pol[a,b], Erika Vacchelli[a,b], Pierre-Laurent Puig[j,n], and Guido Kroemer 🔘[a,b,n]

aCentre de Recherche des Cordeliers, Equipe Labellisée Par la Ligue Contre le Cancer, Université Paris Cité, Sorbonne Université, Inserm U1138, Institut Universitaire de France, Paris, France; bMetabolomics and Cell Biology Platforms, Villejuif, France; cFaculty of Medicine Kremlin Bicêtre, Université Paris Saclay, Le Kremlin Bicêtre, France; dInstitute of Preventive Veterinary Medicine, Sichuan Agricultural University, Chengdu, Sichuan, China; eDepartment of Chemical, Biological, Pharmaceutical and Environmental Sciences, University of Messina, Messina, Italy; fLaboratory of Proliferation, Stress and Liver Physiopathology, Centre de Recherche des Cordeliers, INSERM, Sorbonne Université, Université Paris Cité, Paris, France; gDepartment of Medical, Surgical and Health Sciences, University of Trieste, Trieste, Italy; hInstitut National de la Santé Et de la Recherche Medicale (INSERM) U1015 and Equipe Labellisée–Ligue Nationale Contre le Cancer, Villejuif, France; iAix Marseille Univ, IRD, AP-HM, MEPHI, IHU Méditerranée Infection, Marseille, France; jCentre de Recherche des Cordeliers, Equipe Labélisée Ligue Contre le Cancer, Sorbonne Université, Université Paris Cité, INSERM, Paris, France; kCenter of Clinical Investigations BIOTHERIS, INSERM CIC1428, Gustave Roussy, Villejuif, France; lInstitut National de la Santé Et de la Recherche Médicale, UMR1015, Gustave Roussy, Villejuif, France; mGustave Roussy Cancer Center, Villejuif, France; nInstitut du Cancer Paris CARPEM, APHP. Hôpital Européen Georges Pompidou, AP-HP, Paris, France

ABSTRACT

Formyl peptide receptor-1 (FPR1) is a pattern recognition receptor that is mostly expressed by myeloid cells. In patients with colorectal cancer (CRC), a loss-of-function polymorphism (rs867228) in the gene coding for FPR1 has been associated with reduced responses to chemotherapy or chemoradiotherapy. Moreover, rs867228 is associated with accelerated esophageal and colorectal carcinogenesis. Here, we show that dendritic cells from $Fpr1^{-/-}$ mice exhibit reduced migration in response to chemotherapy-treated CRC cells. Moreover, $Fpr1^{-/-}$ mice are particularly susceptible to chronic ulcerative colitis and colorectal oncogenesis induced by the mutagen azoxymethane followed by oral dextran sodium sulfate, a detergent that induces colitis. These experiments were performed after initial co-housing of $Fpr1^{-/-}$ mice and wild-type controls, precluding major Fpr1-driven differences in the microbiota. Pharmacological inhibition of Fpr1 by cyclosporin H also tended to increase intestinal oncogenesis in mice bearing the Apc^{Min} mutation, and this effect was reversed by the anti-inflammatory drug sulindac. We conclude that defective FPR1 signaling favors intestinal tumorigenesis through the modulation of the innate inflammatory/immune response.

Introduction

Colorectal cancer (CRC) is one of the most prevalent malignancies worldwide and represents 10% of all cancer types.[1,2] However, when detected at an early stage, CRC is cured in 9 out of 10 cases. Several risk factors are known to be associated with CRC initiation and progression, including old age, obesity, red meat consumption, chronic intestinal inflammation, and genetic alterations.[1,3] Additionally, by 2040, the worldwide burden of CRC is projected to increase to 3.2 million new cases and 1.6 million deaths with an increasing incidence in countries with a high or very high income[4].

Formyl peptide receptors (FPRs) are pattern recognition receptors known to play important roles in diverse physiological processes, including host defense and inflammation.[5] FPRs recognize peptides bearing a particular post-translational modification, namely N-formylation, that is only catalyzed by enzymes present in bacteria and in mitochondria. Hence, these N-formylated peptides consist of microbial pathogen-associated molecular patterns (MAMPs) or danger-associated molecular patterns (DAMPs) derived from dying cells spilling mitochondrial content.[6,7] Furthermore, FPR1 recognizes non-formylated proteins such as (i) cathepsin G,[8] (ii) family with sequence similarity 19 (chemokine (C–C motif)-like), member A4 (FAM19A4),[9] and (iii) annexin A1 (ANXA1) that is released from the cytosolic compartment of dying and dead cells, hence constituting yet another DAMP.[7,10]

We previously showed that a loss-of-function polymorphism in *FPR1*, rs867228, with an allelic frequency of ~20% across all ethnic groups, is associated with poor responses to anthracycline-based adjuvant chemotherapy in two distinct cohorts of breast cancer and one cohort of CRC patients.[11,12] Another group confirmed that rs867228 is associated with poor prognosis in patients with locally advanced rectal cancer treated with neoadjuvant chemoradiotherapy.[13,14] Homo- or heterozygous presence of the minor allele in rs867228 causes the anticipated manifestation (by ~6 y) of luminal B breast

cancer.[15] Homozygous presence of the minor allele of rs867228 (which affects ~4% of the population) is associated with the earlier diagnosis of gastrointestinal cancers, in particular esophagus and colorectal carcinomas, by ~5 y.[16,17] Of note, peripheral blood mononuclear cells from individuals bearing rs867228 either in heterozygosity or in homozygosity show a reduced interaction with anthracycline-treated dying tumor cells in microfluidic chambers.[11,18] The FPR1 ligand involved in this interaction turned out to be ANXA1.[11]

Echoing the aforementioned clinical observations, $Fpr1^{-/-}$ and $Fpr1^{\pm}$ mice were unable to mount a tumor-specific immune response against different tumor cell types (e.g., fibrosarcoma, pulmonary adenocarcinoma, malignant mammary tumor) treated with immunogenic cell death inducers (e.g., cyclophosphamide, doxorubicin, mitoxantrone, and oxaliplatin). Moreover, in a model of carcinogen-induced mammary carcinoma, female $Fpr1^{-/-}$ mice developed mammary carcinoma earlier than wild-type mice.[11,16] Exhaustive phenotyping of the immune populations infiltrating the tumor bed upon chemotherapy demonstrated that Fpr1 is required for the very initial steps leading to antitumoral immunity. Defects of Fpr1 were linked to the suboptimal activation of dendritic cells (DCs) belonging to the type 1 conventional DC (cDC1) subset. The latter failed to position themselves in the proximity of ANXA1-releasing dying cancer cells.[16,18] Altogether, these experiments established that Fpr1 plays a cardinal role in the establishment of cancer immunosurveillance.

As mentioned above, patients with homozygosity in rs867228 tend to develop colorectal cancers several years earlier than patients lacking rs867228.[16,17] However, we have not yet addressed the question as to whether FPR1 would affect the immunosurveillance of CRC. Here, we provide evidence that genetic or pharmacological inhibition of FPR1 facilitates intestinal oncogenesis in inflammation-driven and genetic models.

Results

Fpr1 facilitates the migration of dendritic cells toward dying CRC cells

Bone-marrow derived dendritic cells (BMDCs) were obtained from C57Bl/6 mice harboring functional $Fpr1$ alleles ($Fpr1^{+/+}$ or wild type, WT) or lacking one ($Fpr1^{\pm}$) or both alleles of $Fpr1$ ($Fpr1^{-/-}$). To examine their migratory capacity, BMDCs were placed on top of microporous membranes and their migration through these membranes toward lower chambers was monitored by measuring impedance in a specialized device (see Materials & Methods). Migration was stimulated by placing the supernatant of MC38 CRC cells (syngeneic in immunocompetent C57Bl/6 mice) that were left untreated (control) or transiently treated with the chemotherapeutic agent oxaliplatin (OXA) into the lower chambers (Figure 1a). As compared to supernatants from untreated MC38 cells, supernatants from OXA-treated MC38 cells stimulated migration of WT BMDCs. This migration-stimulatory effect was attenuated when $Fpr1^{+/+}$ BMDCs were replaced by $Fpr1^{\pm}$ and $Fpr1^{-/-}$ BDMCs, the latter exhibiting the lowest propensity for migration (Figure 1b–d). Similarly, $Fpr1^{-/-}$ BDMCs demonstrated reduced migration abilities even at basal state (i.e., in the presence of supernatants

from untreated MC38 cells) (Figure 1b,c). However, the specific response of BMDCs to cell death (i.e., the difference of migration in response of OXA-treated versus untreated CRC cells) was strongly compromised by the absence of Fpr1 (Figure 1d). These findings suggest that Fpr1 governs the spatial relationship between myeloid and CRC cells, motivating us to investigate the impact of Fpr1 on intestinal carcinogenesis and tumor progression.

Effects of FPR1 on inflammation-induced CRC

To investigate the potential effects of $Fpr1$ deficiency, we turned to an inflammation-induced model of CRC caused by a single intraperitoneal (i.p.) administration of the mutagen azoxymethane (AOM) followed by oral dextran sodium sulfate (DSS), a detergent that induces colitis[19,20]. This colon-carcinogenic protocol was applied to mice bearing a WT, $Fpr1^{\pm}$, or $Fpr1^{-/-}$ genotype. Of note, we performed co-housing of mice with the three genotypes before the initiation of the protocol (Figure 2a)[21] thus minimizing possible differences in gut microbiota that might have arisen from defects of $Fpr1$, as determined by 16S sequencing of fecal material (collected before AOM injection and after one cycle of DSS). Hierarchical Cluster Analysis (HCA, Figure 2b) and non-supervised Principal Coordinate Analysis (PCoA, Figure 2c), both employed with Bray-Curtis distance, failed to detect major differences in the overall microbiota composition among $Fpr1$ genotypes, thus confirming the capacity of cohousing to homogenize microbiota structure, irrespective of $Fpr1$ genetic background. PCoA showed that the unique statistical difference in microbiota composition was among AOM+DSS and control mice (Figure 2c). The supervised Partial Least Square Discriminant Analysis (PLS-DA, Figure 2d) revealed differences in microbiota composition, especially for $Fpr1^{+/+}$ AOM+DSS treated mice. Thus, variable of importance in projection (VIP) scores (Figure 2e) showed that 7 out of 19 differentially abundant species (most importantly *Parabacteroides goldstenii* and *Eubacterium siraeum*) had higher relative abundances in this group. Interestingly, $Fpr1^{-/-}$ mice at baseline showed a minor shift in the abundance of *Parasutterella excrementihominis* and *Lactobacillus reuteri*, which are species having the lowest relative abundance in $Fpr1^{+/+}$ AOM+DSS mice. Among the 44 bacteria species evidenced by the VIP plot (Figure 2e), 18 were significant without FDR and 10 were significant after a Benjamini–Hochberg two-stages 10% FDR (Supplemental Table S1), indicating that only a minority of the identified bacterial species (10 out of 441 species or 2.3%) differed in their relative abundance. Additionally, in contrast to a prior report that did not perform cohousing,[22] we did not find any significant difference in colon inflammation (indicated by weight loss, Fig S2B, diarrhea or rectal bleeding, data not shown) between $Fpr1$-proficient and -deficient mice (Figure 2c–e). For colorectal carcinogenesis, we continued the experiment by supplying two additional cycles of oral DSS (Figure 3a). $Fpr1^{-/-}$ mice developed more
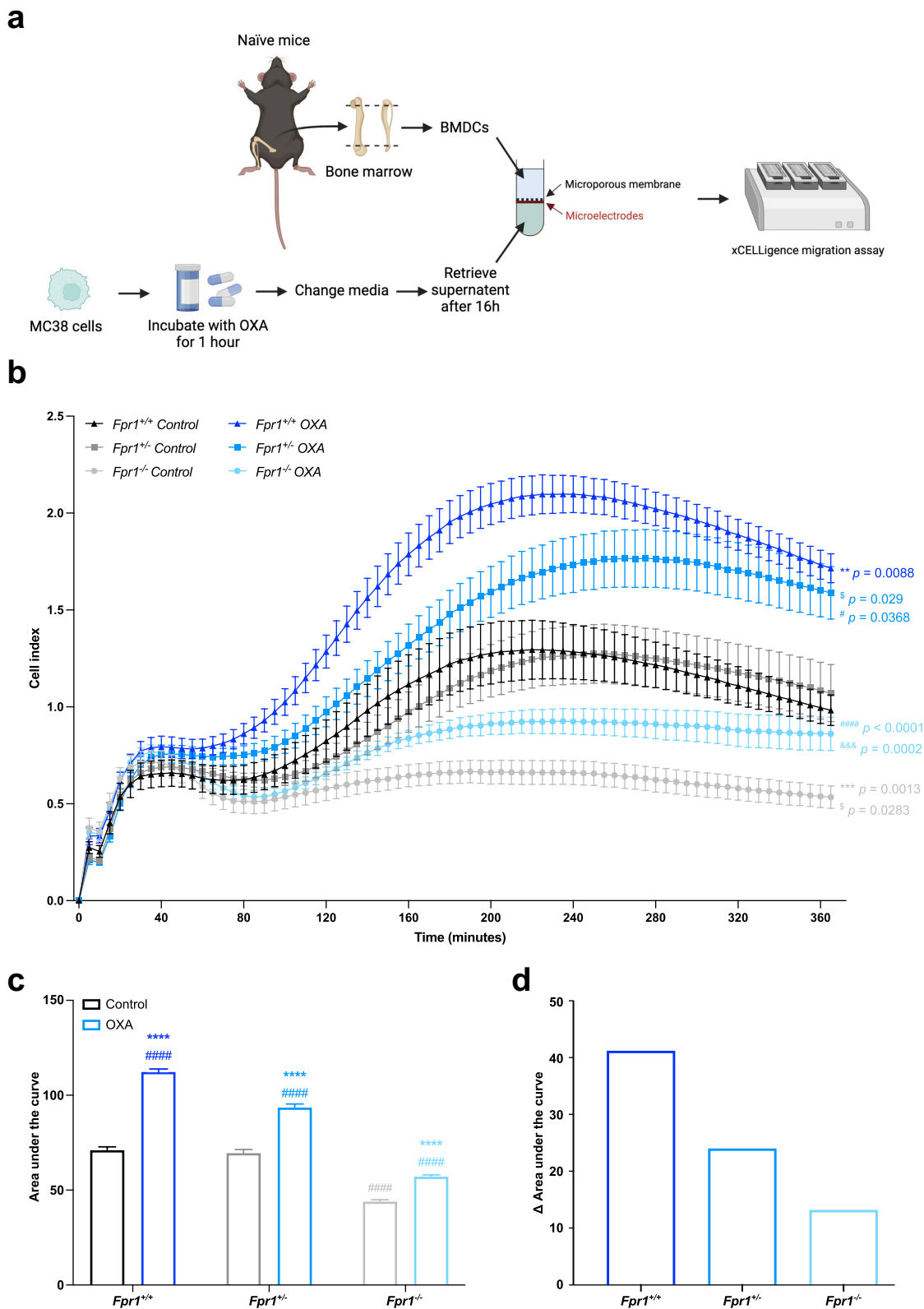
Figure 1. *Fpr1* defects induce a migration defect. Notes: 3×10^4 MC38 colon carcinoma cells were treated with oxaliplatin (OXA) or left untreated. After 1 h, treatment media was replaced by fresh media. After 16 h of culture, supernatants were retrieved and used as chemoattractant. Bone-marrow derived dendritic cells (BMDCs) were isolated and cultured for 7 d in granulocyte-macrophage colony-stimulating factor containing media. The migration of 6×10^4 BMDCs from $Fpr1^{-/-}$, $Fpr1^{\pm}$, and $Fpr1^{+/+}$ mice toward the chemoattractant was monitored over 24 h. For each condition, at least seven internal replicates are represented. (a) Overall scheme of the experiment. (b) Cell index of BMDCs reaching the compartment containing chemoattractant. Results from a representative experiment are illustrated as mean ± SEM over time. ** $p < 0.01$, *** $p < 0.001$ as compared to $Fpr1^{+/+}$ control mice; $^{\#}p < 0.05$, $^{\#\#\#\#}p < 0.0001$ as compared to $Fpr1^{+/+}$ OXA-treated MC38 cells; $^{\$}p < 0.05$ as compared to $Fpr1^{\pm}$ control mice; $^{\&\&\&}p < 0.005$ as compared to $Fpr1^{\pm}$ OXA-treated MC38 cells. (c) Area under the curve of the panel B. **** $p < 0.0001$ as compared to untreated control mice; $^{\#\#\#\#}p < 0.0001$ as compared to $Fpr1^{+/+}$ control mice. (d) Difference in the area under the curve of OXA-treated and untreated BMDCs.
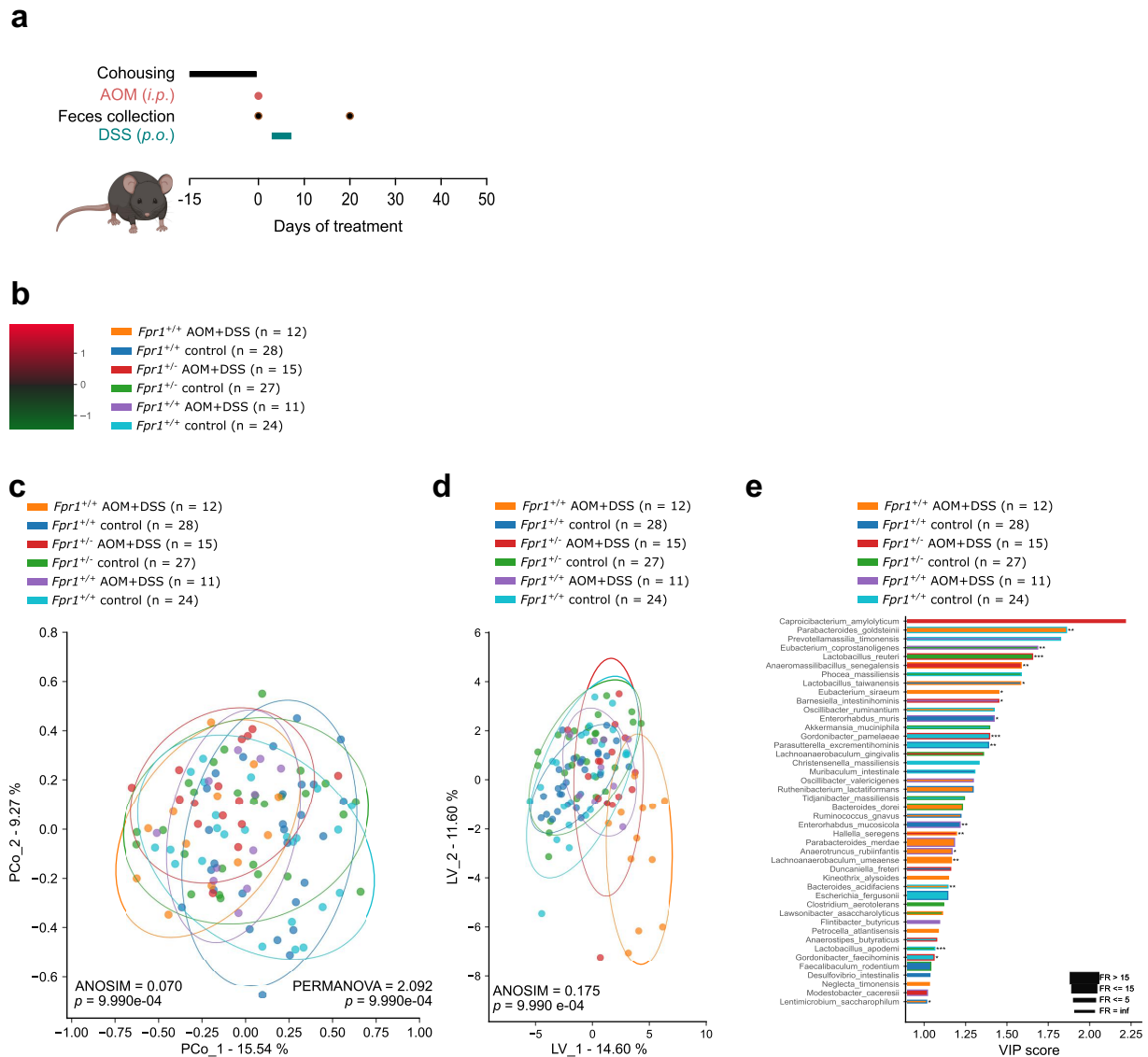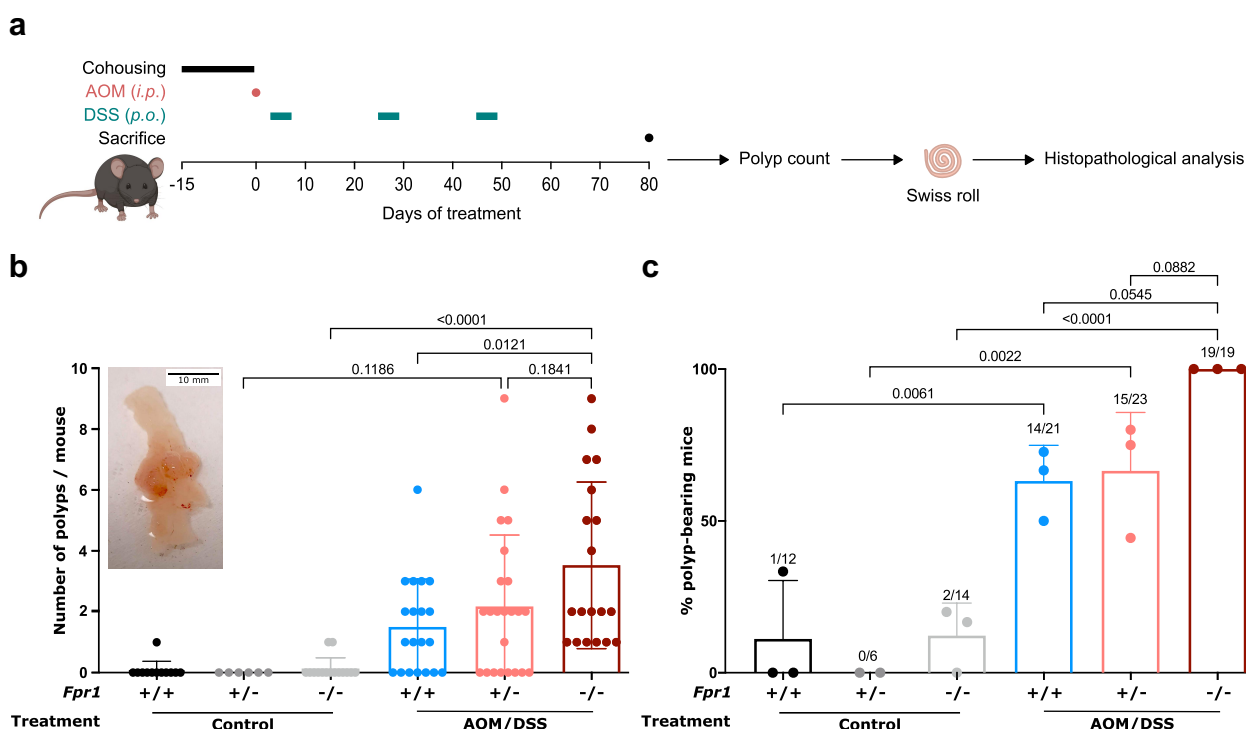
Figure 2. *Fpr1* genotype does not impact microbiota. Notes: After a 2-week-long cohousing period *Fpr1*$^{+/+}$, *Fpr1*$^{±}$, and *Fpr1*$^{-/-}$ C57BL/6 mice were treated (Day 0) with a single intraperitoneal (*i.p.*) injection of azoxymethane (AOM, 10 mg/kg) or with an equivalent volume of PBS (control group), followed by one cycle of 2% dextran sodium sulfate (DSS) in the drinking water for 96 h, starting on day 3 (a). Feces were collected on day 0 and 20 (after AOM injection). (b) Hierarchical cluster analysis (HCA) based on clr-transformed, normalized, and standardized bacterial relative abundances, from low (green) to high (red). On the x-axis are the bacterial species clustered following the Bray-Curtis distance, while on the y-axis the six mice groups considered (*Fpr1*$^{+/+}$ control, blue; *Fpr1*$^{±}$ control, green; *Fpr1*$^{-/-}$ control, cyan; *Fpr1*$^{+/+}$ AOM+DSS, orange; *Fpr1*$^{±}$ AOM+DSS, red; *Fpr1*$^{-/-}$ AOM+DSS, purple). (c) Unsupervised principal coordinate analysis (PCoA) showing beta-diversity difference (ANOSIM and PERMANOVA metrics) among the groups in terms of bacterial species relative abundances, after transformation, normalization, and standardization. Values represent the number of mice for each group. (d) Supervised Partial Least Square Discriminant Analysis (PLS-DA) for the same groups of panel C, beta-diversity measured by ANOSIM. (e) Variable Importance Plot (VIP) shows: (i) discriminant species after PLS-DA in descending order of VIP score (bar length); (ii) the highest relative abundance depending on the cohort (central bar color) and the lowest one (edge bar color); (iii) significant difference after Mann – Whitney U test (non-FDR, *$p \leq 0.05$, ** $p \leq 0.01$; *** $p \leq 0.001$). Results from two pooled independent experiments yielding similar results are illustrated.

macroscopically visible colon polyps (which include various histological lesions such as hyperplasia, adenoma, and carcinomas, though without any visible impact on their size) than *Fpr1*$^{+/+}$ mice (Figure 3b). Notably, all *Fpr1*$^{-/-}$ mice (19 out of 19) developed such lesions, contrasting with 15 out of 23 all *Fpr1*$^{±}$ mice and the relatively low frequency of *Fpr1*$^{+/+}$ mice exhibiting polyps (14/21) (Figure 3c).

A histological examination of Swiss rolls confirmed these macroscopic differences (Figure 4a–d). For this, we evaluated colonic non-neoplasic lesions i) inflammatory cell infiltration, ii) surface epithelium, and crypt injury, as well as iii) colonic

reactive mucosal hyperplasia (Figure 4a–d and Table S1). Altogether, the cumulative histopathological score was increased in *Fpr1*$^{-/-}$ mice as compared to *Fpr1*$^{+/+}$ controls though this result was not significant (Figure 4e and Fig. S1), correlating with the macroscopic evaluation of the polyp count (Figure 4f). We then separately evaluated histologically detectable adenomas and adenocarcinomas, favored by these inflammatory-driven lesions. These malignancies preferentially developed in *Fpr1*-deficient animals rather than in WT controls (Fig. S2). Mice with the *Fpr1*$^{±}$ genotype manifested an intermediate phenotype (Figure 4 and S1).

Figure 3. Fpr1 genotype impacts inflammation-induced neoplasia at the macroscopic level. Notes: After a two-week-long cohousing period *Fpr1*^{+/+}, *Fpr1*[±], and *Fpr1*^{−/−} C57BL/6 mice were treated (Day 0) with a single intraperitoneal (*i.p.*) injection of azoxymethane (AOM, 10 mg/kg) followed by three cycles of 2% dextran sodium sulfate (DSS) in the drinking water for 96 h, starting on day 3 or with an equivalent volume of PBS (control group). All mice were sacrificed at 80 d, when colons were rolled, fixed in formaldehyde, and transferred into ethanol after 24 h. Samples were embedded in paraffin and underwent hematoxylin, eosin, and saffron (HES) staining. Results from three pooled independent experiments yielding similar results are shown as dot plots which indicate means ± SD. *p* values inferior to 0.2 are indicated (Kruskal Wallis and ROUT (Q = 2%) tests). (a) Overall scheme of the experiment. (b) Number of polyps per mouse with a representative picture of a polyp-bearing colon. Each dot represents one mouse. (c) Average percentage of polyp-bearing mice and total number of polyp-bearing mice in three independent experiments, each indicated by one dot. Numbers above the columns indicate the number of mice bearing polyps macroscopically observed among the total number of mice included in each experimental group.

In conclusion, homozygous *Fpr1* deficiency significantly favors colonic reactive mucosal hyperplasia as well as inflammation-induced colon tumorigenesis. It appears improbable that these effects can be attributed to shifts in the microbiota, rather suggesting that they are due to immune system-intrinsic defects in immunosurveillance.

### Effects of Fpr1 on APC[Min/+]-induced cancers

Mice bearing the truncation mutation *Min* (multiple intestinal neoplasia) in codon 850 of the gene *Apc* (adenomatous polyposis coli), referred to as *Apc*[Min/+] mice, show constitutive overactivation of the Wnt pathway leading to intestinal carcinogenesis.[23,24] We treated such mice with the pharmacological Fpr1 antagonist cyclosporin H (CsH) once per week for 8 weeks (*i.p.* at 30 mg/kg/ mouse), alone or in combination with two treatment periods of the non-steroidal anti-inflammatory drug sulindac (Figure 5a), which is known to attenuate intestinal oncogenesis.[25] Of note, sulindac has a pleiotropic effect (on inflammation, proliferation, and Wnt/ß-catenin signaling).[26–28] CsH treatment increased the number of lesions (atypical hyperplasias or intestinal adenomas across the intestine) developing in *Apc*[Min/+] animals as compared to untreated *Apc*[Min/+] mice. This pro-tumorigenic CsH effect was abrogated by simultaneous sulindac treatment (Figure 5b,c), suggesting that Fpr1 inhibition contributes to the manifestation

of atypical hyperplasias or intestinal adenomas via proinflammatory effects.

Discussion

Homozygous presence of rs867228, a loss-of-function polymorphism in *FPR1*, is associated with the precocious manifestation of gastrointestinal cancers, in particular esophagus and colorectal carcinomas. Here, we investigated the impact of genetic or pharmacological inhibition of Fpr1 on experimental intestinal neoplasia developing in mice. We found that Fpr1 inhibition enhanced the propensity of mice to intestinal oncogenesis in two models, namely, (i) carcinogen and inflammation-driven (AOM/DSS) colorectal oncogenesis and (ii) *Apc*[Min]-induced tumorigenesis affecting the small intestine. Although it is tempting to assume that these effects are due to deficient immunosurveillance, the mechanistic underpinnings of these phenomena remain to be elucidated.

In mice, the knockout of *Fpr1* has ambiguous effects on the control of microbial infections as well as on noninfectious diseases, which might explain – at the theoretical level – why loss-of-function variants of *FPR1* constitute an advantage for a population of individuals exposed to a heterogeneous panel of external and internal disease drivers. Thus, the knockout of *Fpr1* increases bacterial burden,
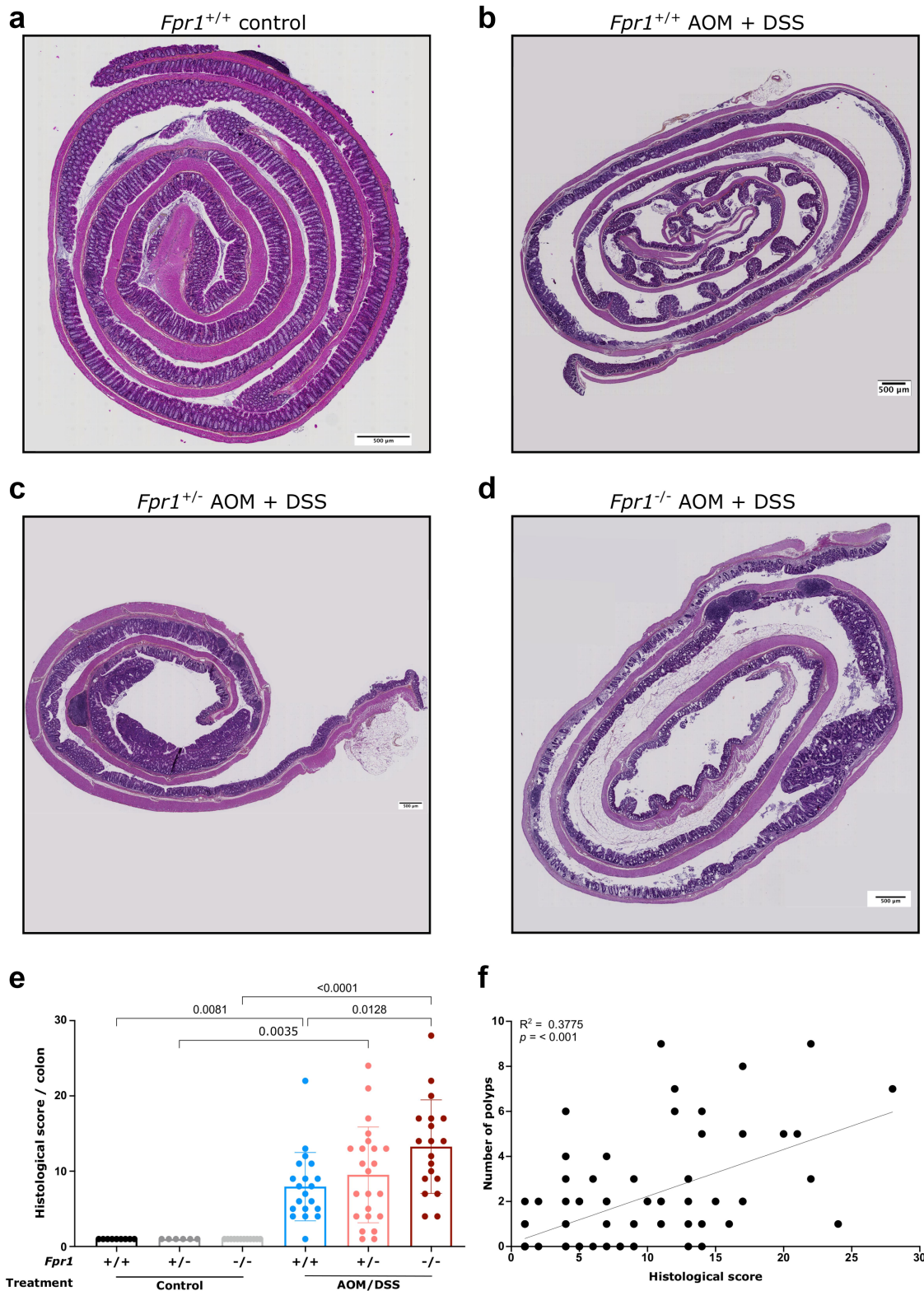
Figure 4. Absence of *Fpr1* increases chronic ulcerative colitis lesions and favors colon tumorigenesis. Notes: After a two-week-long cohousing period *Fpr1*$^{+/+}$, *Fpr1*$^{\pm}$ and *Fpr1*$^{-/-}$ C57BL/6 mice were treated (Day 0) with a single intraperitoneal (*i.p.*) injection of azoxymethane (AOM, 10 mg/kg) or with an equivalent volume of PBS (control group), followed by three cycles of 2% DSS in the drinking water for 96 h, starting on day 3. At 80 d colons were recovered in formalin and transferred in ethanol after 24 h. Samples were included in paraffin and then hematoxylin, eosin, and saffron (HES) stained. Representative sections are shown for untreated *Fpr1*$^{+/+}$(a) and treated *Fpr1*$^{+/+}$(b), *Fpr1*$^{\pm}$(c), and *Fpr1*$^{-/-}$(d) C57BL/6 mice. (e) Total histological score per colon, calculated as follows: inflammation score (severity × extent) + crypt damage (severity × extent) + hyperplasia (severity × extent). (f) Simple linear regression curve between the number of polyps observed macroscopically and histological score from the AOM/DSS-treated groups, irrespective of the genotype, are depicted. R and *p* values were calculated using spearman correlation. Results from three pooled independent experiments yielding similar results are shown. Dot plots indicate means ± SD. *p* values inferior to 0.2 are indicated (one-way ANOVA, Tukey multiple comparison test).
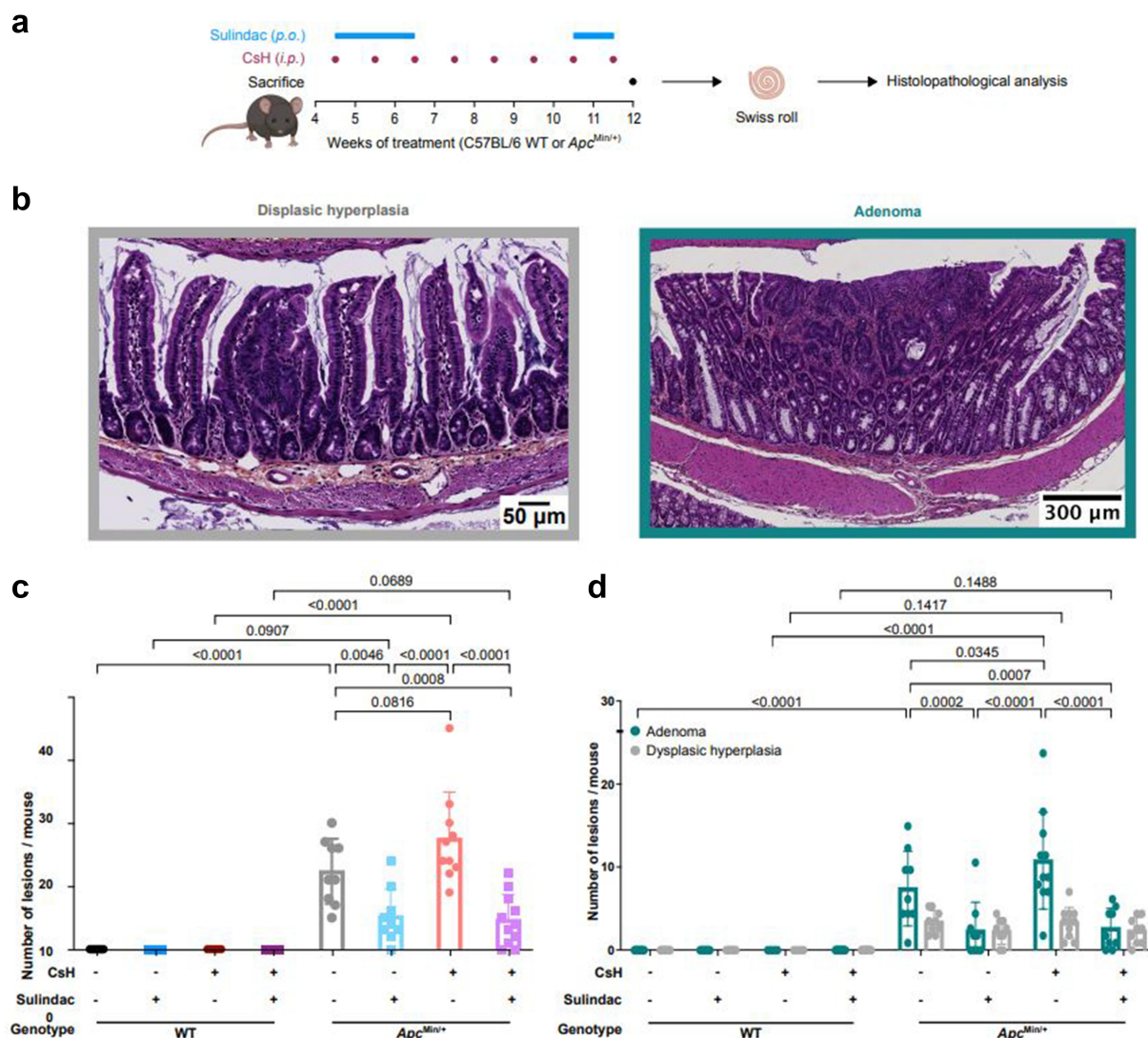
Figure 5. Antagonism of *Fpr1* impacts intestinal tumorigenesis in the spontaneous *APC*^{*Min/+*} model. Notes: *APC*^{*Min/+*} (heterozygous) or WT mice were treated weekly with cyclosporin H (CsH, *i.p.* 30 mg/kg/mouse), while the non-steroidal anti-inflammatory drug sulindac was administered by switching from regular diet to one containing 300 ppm sulindac. (a) Overall scheme of the experiment. (b) Enlarged windows of representative pre-neoplastic lesions: i) atypical hyperplasia, a well-circumscribed intra-epithelial proliferation of densely packed enterocytes and ii) adenoma, a benign well-demarcated neoplasm extending beyond the confinement of the intestinal mucosa. (c and d) Number of lesions per mouse. Results from four independent experiments yielding similar results are illustrated. Histograms illustrate means ± SD. *p* values lower than 0.2 are indicated (one-way ANOVA, Tukey multiple comparison test).

inflammation, and mortality in murine models of pneumococcal meningitis (where *Streptococcus pneumoniae* is injected into the subarachnoid space)[29], Listeriosis (where *Listeria monocytogenes* is administered intravenously) or peritonitis (where pathogenic isolates of *Escherichia coli* are injected *i.p.*)[30], but protects against plague (where *Yersinia pestis* is administered subcutaneously).[31] According to one report, *Fpr1*^{−/−} mice exhibit higher levels of circulating interleukin (IL-) 6, tumor necrosis factor (TNF-) α and chemokine (C-X-C motif) ligand 1 (CXCL1) post-lipopolysaccharide (LPS) challenge, as well as more liver damage indicated by apoptosis and transaminase elevation, as compared to WT controls.[32] However, deletion of *Fpr1* protects against cuprizone-induced demyelination of the corpus callosum and neuroinflammation of the cortex[33] and improves the outcome of traumatic brain injury[34] and transient focal brain ischemia through reduced neuroinflammation.[35] Deletion of *Fpr1* also mitigates lung

damage by aerosolized or intratracheally instilled LPS,[36,37] cigarette smoke,[38,39] intratracheal bleomycin instillation,[40] and bronchiolitis obliterans syndrome induced by allogeneic heterotopic tracheal transplantation.[41]

At the gut level, the *Fpr1* deletion reduces acute colitis induced by one single cycle of oral treatment with DDS[42,43] or intracolonic administration of dinitrobenzene sulfonic acid (DNBS)[44]. However, upon two cycles of DDS, colitis has been reported to be histologically worse with more ulcers in *Fpr1*^{−/−} mice.[43] In our study – which involved three cycles of DDS plus a pretreatment with AOM, the most commonly used model of chemically induced colon carcinogenesis,[45] the *Fpr1* KO did not significantly modulate intestinal inflammation leading to weight loss (Fig S2).

FPR1 and the microbiota exhibit reciprocal effects. Although there are no major changes in the context of a normal diet, *Fpr1*^{−/−} mice on a high fat diet exhibit an altered microbiota as compared to WT mice with an increase in

Rikenellaceae,[46] which, based on rather indirect evidence, might favor colorectal carcinogenesis.[47] Reportedly, the *Fpr1* KO reduces the formation of organized intraluminal structures that encapsulate commensals following acute *Toxoplasma gondii* gastrointestinal infection, correlating with increased microbial translocation, poor commensal containment, and higher mortality.[48] $Fpr1^{-/-}$ mice failed to recruit an anaerobic bacterial consortium including *Akkermansia muciniphila* into the proximity of colonoscopy-induced wounds.[49] The wound closure-promoting effect of *A. muciniphila* requires FPR1 as well as intestinal epithelial-cell-specific nicotinamide adenine dinucleotide phosphate oxidase 1-dependent redox signaling.[49] However, the implication of *A. muciniphila* in AOM/DSS-induced colon carcinogenesis is controversial.[50,51] Daily gavage of *Lactobacillus rhamnosus* GG (LGG) to WT mice increases gastrointestinal motility, and this effect is not seen in $Fpr1^{-/-}$ mice.[52] The *Fpr1* KO reduces intestinal healing of wounds induced by colonoscopy in response to intrarectal administration of LGG.[42] Of note, to exclude the possibility that the absence of Fpr1 might affect intestinal oncogenesis in an indirect fashion (via microbiota shifts) rather than in a (more) direct fashion (via effects on immunosurveillance), $Fpr1^{+/+}$ and $Fpr1^{-/-}$ mice were cohoused before the initiation of treatments with AOM and DSS. In this experimental design, we did not detect any major differences between the microbiota in $Fpr1^{+/+}$ and $Fpr1^{-/-}$ mice subjected to AOM and DSS. At this point, we therefore cannot argue in favor of the hypothesis that Fpr1 would induce CRC-relevant changes in the intestinal microbiota.

Although $Fpr1^{-/-}$ mice did not manifest any major shift in their fecal microbiota compared to their WT controls, it is still possible that they respond differently to carcinogenic effects depending on the microbiota, which clearly modulates inflammation-induced colon carcinogenesis.[53,54] LGG, which acts through FPR1 on gut motility[49] and colon wound closure,[49] limits AOM/DSS-induced colon carcinogenesis.[55] *In vitro* data suggest that the antiangiogenic and inflammation resolving effects of LGG on colon cancer cells are mediated by FPR1.[55] Hence, it will be interesting to study the possibility that the effects of tumor-suppressive bacteria on intestinal carcinogenesis are mediated by FPR1 signaling. Moreover, it appears possible – yet remains to be formally demonstrated – that defects in $Fpr1^{-/-}$ immune cells (such as the reduced migration of $Fpr1^{-/-}$ dendritic cells toward stressed or dying CRC cells) account for inadequate anticancer immune responses in a microbiota-independent fashion.

Irrespective of these uncertainties, it appears that FPR1 deficiency favors intestinal oncogenesis. These findings suggest that the association of rs867228 with early diagnosis of gastrointestinal malignancies reflects a cause–effect relationship.

Material and methods

Chemicals

Cyclosporin H (#HY-P1122) was purchased from MedChem. Dextran sodium sulfate (#42867) and azoxymethane (#A5486) were provided by Sigma Aldrich. Pierce™ 16% formaldehyde methanol-free (#28908) was purchased from Thermo Fisher Scientific. The Haemalum–Shorr staining solution (#720–0330), Saffron (#720–0184) and Ethanol absolute (#20821.310 or #20821.365) were provided by VWR. Phosphate buffered saline (#100123, Gibco) was purchased from Gibco. Sub-X clearing medium (#3803672), paraffin (#39V2001 or #39601006), Rabbit HRP PowerVision kit (#PV6119) and BOND Epitope dewax solution (#AR9222) were provided by Leica Biosystem. Eosin-Y aqueous (#6766010) was purchased from MM France.

Animals

Mice were bred and maintained in the animal facilities of the Centre de Recherche des Cordeliers in specific pathogen-free conditions in a temperature-controlled environment with 12-h light/12-h dark cycles and received food and water *ad libitum* with standard diet unless otherwise stated. $Fpr1^{-/-}$ mice were originally produced by Taconic under the commercial name C57BL/6NTac-Fpr1tm1Gao N6. Subsequent breedings were performed in house. Animal experiments followed the Federation of European Laboratory Animal Science Association (FELASA) guidelines and were in compliance with EU Directive 63/2010. Protocols #24973–2020040413162969 v3 and #30574–2021031815209398 v4 were approved by the Charles Darwin Ethical Committee (C2EA–05 registered at the French Ministry of Research).

Inflammation-induced colorectal oncogenesis

Females and males 6- to 10-weeks-old were used in these experiments. 6- to 10-week-old wild-type C57BL/6J female mice were obtained from Envigo. After a two-week cohousing period, $Fpr1^{+/+}$, $Fpr1^{\pm}$, and $Fpr1^{-/-}$ mice were randomized and treated (Day 0) with a single intraperitoneal (*i.p.*) injection of AOM (10 mg/kg) or with an equivalent volume of vehicle (PBS, control group). Three days later, animals from the treated group received 2% DSS in the drinking water for 96 h, followed by a 2-week rest period without DSS, then another 96-h cycle of 2% DSS followed by a second 2-week rest period and, at last, a final 96-h cycle of 2% DSS. All mice were sacrificed by cervical dislocation 80 d after AOM administration. A longitudinal analysis of fraction of initial weight data was performed by linear mixed-effect modeling (https://kroemerlab.shinyapps.io/TumGrowth/).[56]

APC^{Min/+} spontaneous intestinal oncogenesis

4-week-old females and males were used in these experiments. $APC^{Min/+}$ mice or WT littermates were treated *i.p.* weekly with cyclosporin H (CsH, 30 mg/kg/mice) or with an equivalent volume of vehicle (PBS), while sulindac was administered by switching from regular diet to that containing 300 ppm sulindac. All mice were sacrificed by cervical dislocation at 12 weeks (8 weeks after treatment initiation), and tissues from the small intestine and colon were harvested.

Swiss rolls

Following sacrifice, the ileum, jejunum, duodenum, or colon were excised and processed as previously described.[57] Briefly, the entire length of the tissue was unraveled, cut open longitudinally along its main axis, and washed with PBS. Subsequently, the tissue was macroscopically inspected for the presence of macroscopic protrusions (referred to as polyps), with the luminal side face up, and rolled from the proximal to distal section on a needle from which the eye was cut. The Swiss rolls were then fixed using a minuten pin in 4% formaldehyde for 24 h at 4°C then transferred until paraffin embedding into a cassette in 70% ethanol at 4°C.

Histology

About 5-μm thick sections were performed with a microtome. Swiss roll paraffin-embedded tissue sections underwent either hematoxylin, eosin, and saffron (HES) as previously described.[57] At last, each slide was scanned at a resolution of 0,22 μm per pixel using a 20× objective of the Zeiss Axio Scan Z1 slide scanner and visualized using the QuPath-0.2.3 software.

Histopathological analysis

The histopathological evaluation of HES-stained mouse intestinal tissue sections was conducted on Whole-Slide Images (WSI) in the QuPath-0.2.3 digital pathology software.[58] To ensure reproducible microscopic findings, the description, and diagnosis of mouse intestinal proliferative and nonproliferative lesions reported in the present work followed the most recent and accepted consensual terminology used in mouse pathology, as published by international committees and experts.[59–61] Researchers performing the histological assessment (JLN and PC) were blinded to sample identity at the time of the analysis.

Statistical analysis of ex vivo experiments

Multiple comparisons of the number of polyps or adenomas were conducted using a one- or two-way ANOVA Tukey's multiple comparison test. Multiple comparisons of histological scores were performed using Dunn's multiple comparison test.

Microbiota analysis

Mice feces were collected on day 0 and 20 (after AOM injection) and frozen at −80°C. DNA extraction and 16S rRNA sequencing of mouse stools.

Extraction and 16S-targeted sequencing

Samples were extracted by a mechanical treatment performed with powder glass beads acid washed (G4649-500 g Sigma) and 0.5 mm glass beads cell disruption media (Scientific Industries, Inc) using a FastPrep-24™ 5 G Grinder (mpBio) at maximum speed (6.5 m/s) for 90 s. Then the samples were treated through two kinds of lysis methods: method 1 with classical lysis and protease step following by purification on E.Z.N.A Tissue DNA

Kit (Omega bio-tek, Norcross, Etat-Unis) and method 5 using a deglycosylation step and purification on the EZ1 Advanced XL device (Qiagen, Courtaboeuf, France)[62] Samples were first amplified on these two extractions, pooled and barcoded, then sequenced for 16S rRNA sequencing on MiSeq technology (Illumina, Inc, San Diego CA 92,121, USA) with paired end strategy, constructed according to the 16S targeted sequencing Library Preparation (Illumina). For each protocol extraction, metagenomic DNA was amplified for the 16S "V3-V4" regions by PCR for 45 cycles, using the Kapa HiFi Hotstart ReadyMix 2× (Kapa Biosystems Inc, Wilmington, MA, USA), and the surrounding conserved region V3_V4 primers with overhang adapters (FwOvAd_341F TCGTCGGCAGCGTCAGATGTGTATAAGAGACAGCCT-ACGGGNGGCWGCAG; RevOvAd_785R GTCTCGTGGGCTCGGAGATGTGTATAAGAGACAGGA-CTACHVGGGTATCTAATCCAfter purification on AMPure beads (Beckman Coulter Inc, Fullerton, CA, USA), concentration was measured using High-sensitivity Qubit technology (Beckman Coulter Inc, Fullerton, CA, USA) and dilution to 3.5 ng/μl was performed. At this step, the library of protocol 1 was pooled volume to volume to the library of protocol 5 and Illumina sequencing adapters and dual-index barcodes were added to the amplicon. After purification on AMPure beads (Beckman Coulter Inc, Fullerton, CA, USA), the first library was pooled with 95 multiplexed samples and the second library with 41 multiplexed samples. The global concentration was quantified by a Qubit assay with the high-sensitivity kit (Life Technologies, Carlsbad, CA, USA). Before loading for sequencing on MiSeq (Illumina Inc, San Diego, CA, USA), the pool was diluted at 8 pM. Automated cluster generation and paired-end sequencing with dual index reads was performed in a single 39-h run in a 2×250 bp. The paired reads were filtered according to the read qualities. The raw data were configured in FASTQ files for R1 and R2 reads.

Bioinformatic analysis

Raw FASTQ files were analyzed with DADA2 pipeline v.1.14 for quality check and filtering (sequencing errors, denoising, and chimera detection) on a Workstation Fujitsu Celsius R940 (Fujitsu, Tokyo, Japan). Filtering parameters were as follows: truncLen = 0, minLen = 100, maxN = 0, maxEE = 2, truncQ = 11, trimLeft = 15. All the other parameters in the DADA2 pipeline for paired-end were left as default. Raw reads (5692773 in total, on average 37,700 per sample) were filtered (1921911 in total, on average 12,727 per sample) and 2503 Amplicon Sequence Variants (ASV) were found. Sample coverage was computed and resulted to be on average higher than 99% for all samples, thus meaning a suitable normalization procedure for subsequent analyses. Bioinformatic and statistical analyses on recognized ASV were performed with Python v.3.8.2. Each ASV sequence underwent a nucleotide Blast using the National Center for Biotechnology Information (NCBI) BLAST software (ncbi-blast-2.3.0) and the latest NCBI 16 S Microbial Database (http://ftp.ncbi.nlm.nih.gov/blast/db/). After blasting, the 2503 ASVs were merged into 441 species (thus excluding sub-species or strain differences), and a matrix of their relative abundances and prevalences was built. Only bacterial species having a prevalence equal to or higher than

20% were considered, thus 118 species were considered for subsequent statistical analyses.

Statistics and reproducibility

Data matrices were first transformed with pseudocount and centered-log-ratio (CLR), then normalized and standardized using QuantileTransformer and StandardScaler methods from Sci-Kit learn package v0.20.3. Normalization using the output_distribution = 'normal' option transforms each variable to a Gaussian-like shaped distribution, whilst the standardization results in each normalized variable having a mean of zero and variance of one. These two steps of normalization followed by standardization ensure the proper comparison of variables with different dynamic ranges, such as bacterial relative abundances, or cytokine levels. For microbiota analysis, measurements of α diversity (within sample diversity) such as Richness and Shannon index, were calculated at species level using the SciKit-learn package v.0.4.1. Exploratory analysis of β-diversity (between sample diversity) was calculated using the Bray-Curtis measure of dissimilarity and represented in Principal Coordinate Analyses (PcoA), along with methods to compare groups of multivariate sample units (analysis of similarities – ANOSIM, permutational multivariate analysis of variance – PERMANOVA) to assess significance in data points clustering. ANOSIM and PERMANOVA were automatically calculated after 999 permutations, as implemented in Sci-Kit learn package v0.4.1. To visualize a non-supervised clusterization as PCoA, we implemented with custom scripts (Python v3.8.2) a Hierarchical Clustering Analysis (HCA) with 'Bray-Curtis' metrics and 'complete linkage' method. We implemented Partial Least Square Discriminant Analysis (PLS-DA) and the subsequent Variable Importance Plot (VIP) as a supervised analysis wherein the VIP values (order of magnitude) are used to identify the most discriminant bacterial species among the cohorts. Bar thickness reports the fold ratio (FR) value of the mean relative abundances for each species among the two cohorts, while an absent border indicates mean relative abundance of zero in the compared cohort. Mann – Whitney U test and p values, without FDR, was used for a fixed sample size as previously described, and Kruskal – Wallis tests were employed to assess significance for pairwise or multiple comparisons, respectively, considering a p value < 0.05 as significant.

Migration assay

3×10^4 MC38 colon carcinoma cells were either treated with 400 µM of oxaliplatin (OXA) or left untreated. After 1 h, treatment media was replaced by fresh media. After 16 h, supernatant was retrieved and used as chemoattractant. Bone-marrow derived dendritic cells (BMDCs) were isolated and cultured for 7 d in RPMI-1640 media with pen/strep, L-glutamine, non-essential amino acids, sodium pyruvate, β-mercaptoethanol, and granulocyte-macrophage colony-stimulating factor as previously described.[63] The migration of 6×10^4 BMDCs from $Fpr1^{-/-}$,

$Fpr1^{\pm}$, and $Fpr1^{+/+}$ mice toward the chemoattractant was followed for 24 h. Longitudinal analysis of square root preprocessed cell index data was performed by linear mixed-effect modeling from 40 to 220 min. Wald test was used to compute p values by testing jointly that both cell migration slopes and intercepts of the transformed cell indexes were the same between treatment groups of interest (https://kroemerlab.shinyapps.io/TumGrowth/).[56] Cell index data are represented on the untransformed original scale alongside the SEM computed at each time point. For each condition, at least seven internal replicates are represented.

Disclosure statement

No potential conflict of interest was reported by the author(s).

Disclosures

JGP is named as inventor on patents for cancer vaccination involving an oncolytic rhabdovirus. These patents have been licensed to Turnstone Biologics of which JGP is a shareholder. GK has been holding research contracts with Daiichi Sankyo, Eleor, Kaleido, Lytix Pharma, PharmaMar, Osasuna Therapeutics, Samsara Therapeutics, Sanofi, Tollys, and Vascage. GK is on the Board of Directors of the Bristol Myers Squibb Foundation France. GK is a scientific co-founder of everImmune, Osasuna Therapeutics, Samsara Therapeutics, and Therafast Bio. GK is on the scientific advisory boards of Hevolution, Institut Servier, and Longevity Vision Funds. GK is the inventor of patents covering therapeutic targeting of aging, cancer, cystic fibrosis, and metabolic disorders. GK's brother, Romano Kroemer, was an employee of Sanofi and now consults for Boehringer-Ingelheim. The funders had no role in the design of the study; in the writing of the manuscript or in the decision to publish the results. LZ, who has held research contracts with Glaxo Smyth Kline, Incyte, Lytix, Kaleido, Innovate Pharma, Daiichi Sankyo, Pilege, Merus, Transgene, 9 m, Tusk, and Roche, was on the Board of Directors of Transgene, is a cofounder of everImmune, and holds patents covering the treatment of cancer and the therapeutic manipulation of the microbiota. PLP is a cofounder of MethysDX PLP has been supported by travel or honoraria from Biocartis, MSD, Pierre Fabre, Roche and Sanofi. The other authors declare no conflicts of interest.

Data availability statement

The raw FASTQ files that support the findings of this study are openly available in NCBI at https://www.ncbi.nlm.nih.gov/bioproject/PRJNA976931/,PRJNA976931.

Abbreviations

AOM	azoxymethane
APC	adenomatous polyposis coli
BMDCs	bone-marrow derived dendritic cells
CRC	colorectal cancer
CsH	cyclosporin H
CTL	cytotoxic T lymphocyte

DCs	dendritic cells
DSS	dextran sodium sulfate
FPR1	formyl peptide receptor 1
HES	hematoxylin, eosin and saffron
i.p.	intraperitoneal
KO	knockout
LGG	lactobacillus rhamnosus GG
MIN	multiple intestinal neoplasia
OXA	oxaliplatin
PFA	paraformaldehyde
SNP	single nucleotide polymorphism
WT	wildtype.

ORCID

Guido Kroemer (iD) http://orcid.org/0000-0002-9334-4405

References

1. Keum N, Giovannucci E. Global burden of colorectal cancer: emerging trends, risk factors and prevention strategies. Nat Rev Gastroenterol Hepatol. 2019;16(12):713–732. doi:10.1038/s41575-019-0189-8.
2. Kuipers EJ, Grady WM, Lieberman D, Seufferlein T, Sung JJ, Boelens PG, van de Velde CJH, Watanabe T. Colorectal cancer. Nat Rev Dis Primers. 2015;1(1):15065. doi:10.1038/nrdp.2015.65.
3. O'Sullivan DE, Sutherland RL, Town S, Chow K, Fan J, Forbes N, Heitman SJ, Hilsden RJ, Brenner DR. Risk factors for early-onset colorectal cancer: A systematic review and meta-analysis. Clin Gastroenterol Hepatol. 2022;20(6):1229–1240.e5. doi:10.1016/j.cgh.2021.01.037.
4. Morgan E, Arnold M, Gini A, Lorenzoni V, Cabasag CJ, Laversanne M, Vignat J, Ferlay J, Murphy N, Bray F, et al. Global burden of colorectal cancer in 2020 and 2040: incidence and mortality estimates from GLOBOCAN. Gut. 2023;72(2):338–344. doi:10.1136/gutjnl-2022-327736.
5. Vacchelli E, Le Naour J, Kroemer G. The ambiguous role of FPR1 in immunity and inflammation. Oncoimmunology. 2020;9 (1):1760061. doi:10.1080/2162402X.2020.1760061.
6. Tucker EJ, Hershman SG, Kohrer C, Belcher-Timme CA, Patel J, Goldberger OA, Christodoulou J, Silberstein J, McKenzie M, Ryan M, et al. Mutations in MTFMT underlie a human disorder of formylation causing impaired mitochondrial translation. Cell Metab. 2011;14(3):428–434. doi:10.1016/j.cmet.2011.07.010.
7. Zhuang Y, Wang L, Guo J, Sun D, Wang Y, Liu W, Xu HE, Zhang C. Molecular recognition of formylpeptides and diverse agonists by the formylpeptide receptors FPR1 and FPR2. Nat Commun. 2022;13(1):1054. doi:10.1038/s41467-022-28586-0.
8. Sun R, Iribarren P, Zhang N, Zhou Y, Gong W, Cho EH, Lockett S, Chertov O, Bednar F, Rogers TJ, et al. Identification of neutrophil granule protein cathepsin G as a novel chemotactic agonist for the G protein-coupled formyl peptide receptor. J Immunol. 2004;173 (1):428–436. doi:10.4049/jimmunol.173.1.428.
9. Wang W, Li T, Wang X, Yuan W, Cheng Y, Zhang H, Xu E, Zhang Y, Shi S, Ma D, et al. FAM19A4 is a novel cytokine ligand of formyl peptide receptor 1 (FPR1) and is able to promote the migration and phagocytosis of macrophages. Cell Mol Immunol. 2015;12(5):615–624. doi:10.1038/cmi.2014.61.
10. Baracco EE, Stoll G, Van Endert P, Zitvogel L, Vacchelli E, Kroemer G. Contribution of annexin A1 to anticancer immunosurveillance. Oncoimmunology. 2019;8(11):e1647760. doi:10.1080/2162402X.2019.1647760.
11. Vacchelli E, Ma Y, Baracco EE, Sistigu A, Enot DP, Pietrocola F, Yang H, Adjemian S, Chaba K, Semeraro M, et al. Chemotherapy-induced antitumor immunity requires formyl peptide receptor 1. Science. 2015;350(6263):972–978. doi:10.1126/science.aad0779.
12. Vacchelli E, Enot DP, Pietrocola F, Zitvogel L, Kroemer G. Impact of pattern recognition receptors on the prognosis of breast cancer patients undergoing adjuvant chemotherapy. Cancer Res. 2016;76 (11):3122–3126. doi:10.1158/0008-5472.CAN-16-0294.
13. Chiang SF, Huang KC, Chen WT, Chen TW, Ke TW, Chao KSC. An independent predictor of poor prognosis in locally advanced rectal cancer: rs867228 in formyl peptide receptor 1 (FPR1). Oncoimmunology. 2021;10(1):1926074. doi:10.1080/2162402X.2021.1926074.
14. Chiang SF, Huang KC, Chen WT, Chen TW, Ke TW, Chao KSC. Polymorphism of formyl peptide receptor 1 (FPR1) reduces the therapeutic efficiency and antitumor immunity after neoadjuvant chemoradiotherapy (CCRT) treatment in locally advanced rectal cancer. Cancer Immunol Immunother. 2021;70(10):2937–2950. doi:10.1007/s00262-021-02894-8.
15. Carbonnier V, Le Naour J, Bachelot T, Vacchelli E, Andre F, Delaloge S, Kroemer G. Rs867228 in FPR1 accelerates the manifestation of luminal B breast cancer. Oncoimmunology. 2023;12 (1):2189823. doi:10.1080/2162402X.2023.2189823.
16. Le Naour J, Liu P, Zhao L, Adjemian S, Sztupinszki Z, Taieb J, Mulot C, Silvin A, Dutertre C-A, Ginhoux F, et al. A TLR3 ligand reestablishes chemotherapeutic responses in the context of FPR1 deficiency. Cancer Discov. 2021;11(2):408–423. doi:10.1158/2159-8290.CD-20-0465.
17. Sztupinszki Z, Le Naour J, Vacchelli E, Laurent-Puig P, Delaloge S, Szallasi Z, Kroemer G. A major genetic accelerator of cancer diagnosis: rs867228 in FPR1. Oncoimmunology. 2021;10 (1):1859064. doi:10.1080/2162402X.2020.1859064.
18. Ma Y, Adjemian S, Yang H, Catani JP, Hannani D, Martins I, Michaud M, Kepp O, Sukkurwala AQ, Vacchelli E, et al. ATP-dependent recruitment, survival and differentiation of dendritic cell precursors in the tumor bed after anticancer chemotherapy. Oncoimmunology. 2013;2(6):e24568. doi:10.4161/onci.24568.
19. Angelou A, Andreatos N, Antoniou E, Zacharioudaki A, Theodoropoulos G, Damaskos C, Garmpis N, Yuan C, Xiao W, Theocharis S, et al. A novel modification of the AOM/DSS model for inducing intestinal adenomas in mice. Anticancer Res. 2018;38 (6):3467–3470. doi:10.21873/anticanres.12616.
20. Parang B, Barrett CW, Williams CS. AOM/DSS model of colitis-associated cancer. Methods Mol Biol. 2016;1422:297–307.
21. Robertson SJ, Lemire P, Maughan H, Goethel A, Turpin W, Bedrani L, Guttman DS, Croitoru K, Girardin SE, Philpott DJ, et al. Comparison of co-housing and littermate methods for microbiota standardization in mouse models. Cell Rep. 2019;27(6):1910–1919.e2. doi:10.1016/j.celrep.2019.04.023.
22. Li SQ, Su N, Gong P, Zhang HB, Liu J, Wang D, Sun Y-P, Zhang Y, Qian F, Zhao B, et al. The expression of formyl peptide receptor 1 is

correlated with tumor invasion of human colorectal cancer. Sci Rep. 2017;7(1):5918. doi:10.1038/s41598-017-06368-9.

23. Moser AR, Luongo C, Gould KA, McNeley MK, Shoemaker AR, Dove WF. ApcMin: a mouse model for intestinal and mammary tumorigenesis. Eur J Cancer. 1995;31(7–8):1061–1064. doi:10.1016/0959-8049(95)00181-H.

24. Su LK, Kinzler KW, Vogelstein B, Preisinger AC, Moser AR, Luongo C, Gould KA, Dove WF. Multiple intestinal neoplasia caused by a mutation in the murine homolog of the APC gene. Science. 1992;256(5057):668–670. doi:10.1126/science.1350108.

25. Fletcher R, Tong J, Risnik D, Leibowitz BJ, Wang YJ, Concha-Benavente F, DeLiberty JM, Stolz DB, Pai RK, Ferris RL, et al. Non-steroidal anti-inflammatory drugs induce immunogenic cell death in suppressing colorectal tumorigenesis. Oncogene. 2021;40 (11):2035–2050. doi:10.1038/s41388-021-01687-8.

26. Goldberg Y, Nassif II, Pittas A, Tsai LL, Dynlacht DB, Rigas B, Shiff SJ. The anti-proliferative effect of sulindac and sulindac sulfide on HT-29 colon cancer cells: alterations in tumor suppressor and cell cycle-regulatory proteins. Oncogene. 1996;12:893–901.

27. Haanen C. Sulindac and its derivatives: a novel class of anticancer agents. Curr Opin Investig Drugs. 2001;2:677–683.

28. Lee HJ, Wang XN, Shi DL, Zheng JJ. Sulindac inhibits canonical Wnt signaling by blocking the PDZ domain of the protein Dishevelled. Angew Chem Int Ed Engl. 2009;48(35):6448–6452. doi:10.1002/anie.200902981.

29. Oldekamp S, Pscheidl S, Kress E, Soehnlein O, Jansen S, Pufe T, Wang JM, Tauber SC, Brandenburg L-O. Lack of formyl peptide receptor 1 and 2 leads to more severe inflammation and higher mortality in mice with of pneumococcal meningitis. Immunology. 2014;143(3):447–461. doi:10.1111/imm.12324.

30. Zhang M, Gao JL, Chen K, Yoshimura T, Liang W, Gong W, Li X, Huang J, McDermott DH, Murphy PM, et al. A critical role of formyl peptide receptors in host defense against Escherichia coli. J Immunol. 2020;204(9):2464–2473. doi:10.4049/jimmunol.1900430.

31. Osei-Owusu P, Charlton TM, Kim HK, Missiakas D, Schneewind O. FPR1 is the plague receptor on host immune cells. Nature. 2019;574 (7776):57–62. doi:10.1038/s41586-019-1570-z.

32. Giebeler A, Streetz KL, Soehnlein O, Neumann U, Wang JM, Brandenburg LO, Mukhopadhyay P. Deficiency of formyl peptide receptor 1 and 2 is associated with increased inflammation and enhanced liver injury after LPS-stimulation. PLoS One. 2014;9(6): e100522. doi:10.1371/journal.pone.0100522.

33. Bihler K, Kress E, Esser S, Nyamoya S, Tauber SC, Clarner T, Stope MB, Pufe T, Brandenburg L-O. Formyl peptide receptor 1-mediated glial cell activation in a mouse model of cuprizone-induced demyelination. J Mol Neurosci. 2017;62 (2):232–243. doi:10.1007/s12031-017-0924-y.

34. Fusco R, Gugliandolo E, Siracusa R, Scuto M, Cordaro M, D'Amico R, Evangelista M, Peli A, Peritore AF, Impellizzeri D, et al. Formyl peptide receptor 1 signaling in acute inflammation and neural differentiation induced by traumatic brain injury. Biology (Basel). 2020;9(9):238. doi:10.3390/biology9090238.

35. Li J, Chordia MD, Zhang Y, Zong H, Pan D, Zuo Z. Critical role of FPR1 in splenocyte migration into brain to worsen inflammation and ischemic brain injury in mice. Theranostics. 2022;12 (7):3024–3044. doi:10.7150/thno.57218.

36. Grommes J, Drechsler M, Soehnlein O. CCR5 and FPR1 mediate neutrophil recruitment in endotoxin-induced lung injury. J Innate Immun. 2014;6(1):111–116. doi:10.1159/000353229.

37. Yuan ZC, Zeng N, Liu L, Wang T, Dai LQ, Wang H, Zeng Z-J, Cao Y-F, Zhou Y-F, Xu D, et al. Mitochondrial damage-associated molecular patterns exacerbate lung fluid imbalance via the formyl peptide receptor-1 signaling pathway in acute lung injury. Crit Care Med. 2021;49(1):e53–e62. doi:10.1097/CCM.0000000000004732.

38. Cardini S, Dalli J, Fineschi S, Perretti M, Lungarella G, Lucattelli M. Genetic ablation of the fpr1 gene confers protection from smoking-induced lung emphysema in mice. Am J Respir Cell Mol Biol. 2012;47(3):332–339. doi:10.1165/rcmb.2012-0036OC.

39. Gao L, Zeng N, Yuan Z, Wang T, Chen L, Yang D, Xu D, Wan C, Wen F, Shen Y, et al. Knockout of formyl peptide receptor-1 attenuates cigarette smoke–induced airway inflammation in mice. Front Pharmacol. 2021;12:632225. doi:10.3389/fphar.2021.632225.

40. Leslie J, Millar BJ, Del Carpio Pons A, Burgoyne RA, Frost JD, Barksby BS, Luli S, Scott J, Simpson AJ, Gauldie J, et al. FPR-1 is an important regulator of neutrophil recruitment and a tissue-specific driver of pulmonary fibrosis. JCI Insight. 2020;5(4). doi:10.1172/jci.insight.125937.

41. D'Amico R, Fusco R, Cordaro M, Siracusa R, Peritore AF, Gugliandolo E, Crupi R, Scuto M, Cuzzocrea S, Di Paola R, et al. Modulation of NLRP3 inflammasome through Formyl Peptide Receptor 1 (Fpr-1) pathway as a new therapeutic target in bronchiolitis obliterans syndrome. Int J Mol Sci. 2020;21(6):21. doi:10.3390/ijms21062144.

42. Alam A, Leoni G, Wentworth CC, Kwal JM, Wu H, Ardita CS, Swanson PA, Lambeth JD, Jones RM, Nusrat A, et al. Redox signaling regulates commensal-mediated mucosal homeostasis and restitution and requires formyl peptide receptor 1. Mucosal Immunol. 2014;7(3):645–655. doi:10.1038/mi.2013.84.

43. Farooq SM, Stadnyk AW. Neutrophil infiltration of the colon is independent of the FPR1 yet FPR1 deficient mice show differential susceptibilities to acute versus chronic induced colitis. Dig Dis Sci. 2012;57(7):1802–1812. doi:10.1007/s10620-012-2082-y.

44. Di Paola R, Fusco R, Gugliandolo E, D'Amico R, Cordaro M, Impellizzeri D, Perretti M, Cuzzocrea S. Formyl peptide receptor 1 signalling promotes experimental colitis in mice. Pharmacol Res. 2019;141:591–601. doi:10.1016/j.phrs.2019.01.041.

45. Neufert C, Becker C, Neurath MF. An inducible mouse model of colon carcinogenesis for the analysis of sporadic and inflammation-driven tumor progression. Nat Protoc. 2007;2 (8):1998–2004. doi:10.1038/nprot.2007.279.

46. Wollam J, Riopel M, Xu YJ, Johnson AMF, Ofrecio JM, Ying W, El Ouarrat D, Chan LS, Han AW, Mahmood NA, et al. Microbiota-produced N-Formyl peptide fMLF promotes obesity-induced glucose intolerance. Diabetes. 2019;68(7):1415–1426. doi:10.2337/db18-1307.

47. Terasaki M, Uehara O, Ogasa S, Sano T, Kubota A, Kojima H, Tanaka T, Maeda H, Miyashita K, Mutoh M, et al. Alteration of fecal microbiota by fucoxanthin results in prevention of colorectal cancer in AOM/DSS mice. Carcinogenesis. 2021;42(2):210–219. doi:10.1093/carcin/bgaa100.

48. Molloy MJ, Grainger JR, Bouladoux N, Hand TW, Koo LY, Naik S, Quinones M, Dzutsev A, Gao J-L, Trinchieri G, et al. Intraluminal containment of commensal outgrowth in the gut during infection-induced dysbiosis. Cell Host & Microbe. 2013;14 (3):318–328. doi:10.1016/j.chom.2013.08.003.

49. Alam A, Leoni G, Quiros M, Wu H, Desai C, Nishio H, Jones RM, Nusrat A, Neish AS. The microenvironment of injured murine gut elicits a local pro-restitutive microbiota. Nat microbiol. 2016;1 (2):15021. doi:10.1038/nmicrobiol.2015.21.

50. Wang F, Cai K, Xiao Q, He L, Xie L, Liu Z. Akkermansia muciniphila administration exacerbated the development of colitis-associated colorectal cancer in mice. J Cancer. 2022;13 (1):124–133. doi:10.7150/jca.63578.

51. Wang L, Tang L, Feng Y, Zhao S, Han M, Zhang C, Yuan G, Zhu J, Cao S, Wu Q, et al. A purified membrane protein from Akkermansia muciniphila or the pasteurised bacterium blunts colitis associated tumourigenesis by modulation of CD8 + T cells in mice. Gut. 2020;69(11):1988–1997. doi:10.1136/gutjnl-2019-320105.

52. Chandrasekharan B, Saeedi BJ, Alam A, Houser M, Srinivasan S, Tansey M, Jones R, Nusrat A, Neish AS. Interactions between commensal bacteria and enteric neurons, via FPR1 induction of ROS, increase gastrointestinal motility in mice. Gastroenterology. 2019;157(1):179–192.e2. doi:10.1053/j.gastro.2019.03.045.

53. Hattori N, Niwa T, Ishida T, Kobayashi K, Imai T, Mori A, Kimura K, Mori T, Asami Y, Ushijima T, et al. Antibiotics suppress colon tumorigenesis through inhibition of aberrant DNA methylation in an azoxymethane and dextran sulfate sodium colitis model. Cancer Sci. 2019;110:147–156. doi:10.1111/cas.13880.

54. Lee JG, Eun CS, Jo SV, Lee AR, Park CH, Han DS, Nakano H. The impact of gut microbiota manipulation with antibiotics on colon tumorigenesis in a murine model. PLoS One. 2019;14(12):e0226907. doi:10.1371/journal.pone.0226907.

55. Xu H, Hiraishi K, Kurahara LH, Nakano-Narusawa Y, Li X, Hu Y, Matsuda Y, Zhang H, Hirano K. Inhibitory effects of breast milk-derived lactobacillus rhamnosus Probio-M9 on colitis-associated carcinogenesis by restoration of the gut microbiota in a mouse model. Nutrients. 2021;13(4):1143. doi:10.3390/nu13041143.

56. Enot DP, Vacchelli E, Jacquelot N, Zitvogel L, Kroemer G. TumGrowth: An open-access web tool for the statistical analysis of tumor growth curves. Oncoimmunology. 2018;7(9):e1462431. doi:10.1080/2162402X.2018.1462431.

57. Le Naour J, Montegut L, Joseph A, Garbin K, Vacchelli E, Kroemer G, Pol JG, Maiuri MC. Improved Swiss-rolling method for histological analyses of colon tissue. MethodsX. 2022;9:101630. doi:10.1016/j.mex.2022.101630.

58. Bankhead P, Loughrey MB, Fernandez JA, Dombrowski Y, McArt DG, Dunne PD, McQuaid S, Gray RT, Murray LJ, Coleman HG, et al. QuPath: Open source software for digital pathology image analysis. Sci Rep. 2017;7(1):16878. doi:10.1038/s41598-017-17204-5.

59. Boivin GP, Washington K, Yang K, Ward JM, Pretlow TP, Russell R, Besselsen DG, Godfrey VL, Doetschman T, Dove WF, et al. Pathology of mouse models of intestinal cancer: consensus report and recommendations. Gastroenterology. 2003;124 (3):762–777. doi:10.1053/gast.2003.50094.

60. Nolte T, Brander-Weber P, Dangler C, Deschl U, Elwell MR, Greaves P, Hailey R, Leach MW, Pandiri AR, Rogers A, et al. Nonproliferative and proliferative lesions of the gastrointestinal tract, pancreas and salivary glands of the rat and mouse. J Toxicol Pathol. 2016;29(1_Suppl):1S–125S. doi:10.1293/tox.29.1S.

61. Ward JM, Treuting PM. Rodent intestinal epithelial carcinogenesis: pathology and preclinical models. Toxicol Pathol. 2014;42 (1):148–161. doi:10.1177/0192623313505156.

62. Angelakis E, Bachar D, Henrissat B, Armougom F, Audoly G, Lagier JC, Robert C, Raoult D. Glycans affect DNA extraction and induce substantial differences in gut metagenomic studies. Sci Rep. 2016;6(1):26276. doi:10.1038/srep26276.

63. Boudreau J, Koshy S, Cummings D, Wan Y. Culture of myeloid dendritic cells from bone marrow precursors. J Vis Exp. 2008;17. doi:10.3791/769-v.